Accumulation of dead cells from contact killing facilitates coexistence in bacterial biofilms

Gabi Steinbach,[1] Cristian Crisan,[2,3,4] Siu Lung Ng,[2,3,4] Brian K. Hammer,[2,3,4] and Peter J. Yunker[1]

[1] *School of Physics, Georgia Institute of Technology, Atlanta, GA, USA.*
[2] *School of Biological Sciences, Georgia Institute of Technology, Atlanta, GA, USA.*
[3] *Center for Microbial Dynamics and Infection, Georgia Institute of Technology, Atlanta, GA, USA.*
[4] *Institute for Bioengineering and Biosciences, Georgia Institute of Technology, Atlanta, GA, USA.*

(Dated: May 21, 2021)

Bacterial communities are governed by a wide variety of social interactions, some of which are antagonistic with potential significance for bacterial warfare. Several antagonistic mechanisms, such as killing via the Type VI Secretion System (T6SS), require killer cells to directly contact target cells. The T6SS is hypothesized to be a highly potent weapon, capable of facilitating the invasion and defense of bacterial populations. However, we find that the efficacy of contact killing is severely limited by the material consequences of cell death. Through experiments with *Vibrio cholerae* strains that kill via the T6SS, we show that dead cell debris quickly accumulates at the interface that forms between competing strains, preventing physical contact and thus preventing killing. While previous experiments have shown that T6SS killing can reduce a population of target cells by as much as one-million-fold, we find that as a result of the formation of dead cell debris barriers, the impact of contact killing depends sensitively on the initial concentration of killer cells. Killer cells are incapable of invading or eliminating competitors on a community level. Instead, bacterial warfare itself can facilitate coexistence between nominally antagonistic strains. While a variety of defensive strategies against microbial warfare exist, the material consequences of cell death provide target cells with their first line of defense.

I. INTRODUCTION

Bacteria commonly inhabit biofilms in the form of crowded, surface-attached microbial consortia embedded within a viscous matrix of polymers. Interactions between different bacterial strains and species govern the spatial organization and composition of biofilms [1–3], and ultimately affect the proliferation and survival of individual strains. These interactions can turn deadly. Bacteria have evolved many mechanisms to kill each other within biofilms [4, 5], many of them requiring direct contact between cells [4, 6–9]. One such contact killing mechanism is the broadly prevalent Type VI Secretion System (T6SS) in Gram-negative bacteria [10]. A significant amount of work has produced a detailed picture of the T6SS. Details are emerging of the T6SS structure, toxins, and regulation [10–20]. However, the importance of this lethal activity in natural communities remains unclear [21, 22]. Experiments have primarily focused on the outcome of competitions between T6SS-proficient 'killers' and target strains that lack T6SS activity, but the dynamics of T6SS killing are much less studied [23] (though dynamic simulations have made a number of successful predictions [24–28]). Understanding the impact of the T6SS requires experimental observation of contact killing in microbial communities as a function of time and isolated from other factors. This is a crucial step in assessing the ecological role of contact killing over short and long time scales.

T6SS-mediated killing is widely considered a potent weapon. In biofilms grown from a mixture of T6SS-proficient bacteria and target strains on planar agar pads, killer cells decreased the abundance of target cells by as much as one-million-fold within 3 h [15, 23, 29–31]. Based on these competition assays, the T6SS is hypothesized to play important roles in inter- and intra-strain competition, for example, facilitating invasion of colonized space, elimination of competitors, and defense against invaders and cheaters in biofilms [21, 28, 32–34]. However, in these competition assays T6SS-mediated killing is rarely able to completely eliminate all susceptible target cells, even when killer cells start at numerical advantage (a 10:1 number ratio of killer:target cells is often used) [23, 24, 30, 31, 35]. Further, while the killing rate is typically very high shortly after inoculating competing strains on agar pads, killing nearly halts a few hours later, despite the presence of target cells [23]. This dramatic decrease in killing occurs even when the killer strain expresses a constitutively active T6SS [23]. While some studies report defense mechanisms that mitigate or counteract T6SS attacks [36–41], it is difficult to isolate alterations in T6SS activity over time as developing biofilms become increasingly heterogeneous [42, 43] and constantly change [44–48]: biomass increases, nutrient and oxygen concentrations drop, excreted waste products accumulate, cellular behavior changes due to signaling from secreted public goods. As a result, a detailed picture of how T6SS killing proceeds within biofilms and how T6SS-mediated killing rates change over time remains elusive.

Here, we present the spatio-temporal dynamics of T6SS-mediated killing. We used the T6SS-proficient killer strain *Vibrio cholerae* C6706 and mutants of it, which secrete lethal effectors that cause cell death [30, 35, 37, 49–51]. Through microscopy experiments, we show that while T6SS-mediated killing is effective on first

contact between competing strains, surprisingly, killing nearly ceases after a few hours due to the accumulation of dead cell debris. Contact killing experiments typically focus on living cells as they measure the number of surviving target cells after a certain time of inoculation [15, 29–31, 39, 52–55]. This approach was fundamental in discovering the deadly effect of T6SS [7], the characteristic spatial structure that emerges from contact killing [2, 24, 26, 28], and microbial defense strategies against T6SS attacks [36–39]. Here, we focus on the role of dead cells and dead cell debris. We confirm that dead cell debris accumulates at the interface between competing strains and eventually prevents contact, thus halts killing. Paradoxically, contact killing may thus play a protective role in biofilms, facilitating the formation and coexistence of separate clonal domains [56, 57].

II. RESULTS

To study how T6SS killing proceeds within biofilms, we optically recorded the spatio-temporal dynamics of biofilms comprising two engineered strains of *V. cholerae*, a model organism for studying the T6SS [7]. These strains are isogenic, and only differ in their T6SS toxins and immunity modules, their ability to express T6SS, and their fluorescent proteins [24]. To isolate the effects of killing from other effects related to changes in biofilm height (which can impact cellular behavior [43]), we grew biofilms in confinement between a lysogeny broth (LB) agar pad and a cover glass (Fig. 1a), which limited vertical growth to less than 6 μm. (See Supplementary Material for details on strains and sample preparation.).

A. Spatio-temporal dynamics

As a first step, using confocal time-lapse microscopy we investigated the temporal dynamics of unidirectional killing: the killer was a T6SS-proficient (T6SS+) *V. cholerae* strain, while the target was a susceptible, T6SS-defective (T6SS-) *V. cholerae* strain. We observed the formation of clonal domains (Fig. 1b) upon reproduction and killing. This phenomenon is reminiscent of domain formation observed in populations of mutual killer strains (i.e, both strains are T6SS+) [24], even though in our experiments one strain - the target strain - was engineered to be defective at T6SS killing. While we observed that domains of the killer strain expanded quickly at early times, domain growth later slowed substantially (Fig. 1b). We quantified the temporal dynamics of mixed populations of killer and target strains (Fig. 1c) by measuring the relative abundance of the fluorescent killer strain in the microscopy images over 15 h, for four different initial ratios of killer and target cells (see Supplementary for further details on image analysis). Note that the mixing ratios do not reflect the relative abundance of killer cells at 0 h. Biofilms were grown from

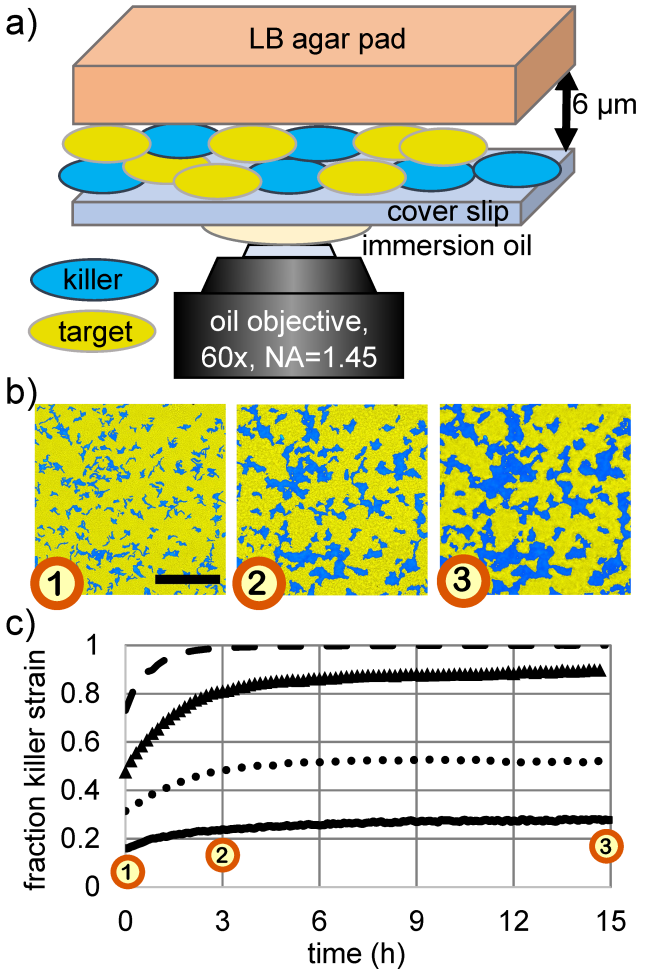

FIG. 1: Contact killing slows substantially over time. a) Cartoon depiction of biofilm samples for imaging. Confinement between an agar pad and a glass cover slide leads to a maximum biofilm thickness of $\sim 6\,\mu$m. b) Fluorescence images of a unidirectional competition between killer cells (blue) and target cells (yellow) at 0 h, 3 h, and 15 h (left to right, respectively). The initial relative abundances were 0.09 killer cells and 0.91 target cells. T6SS-mediated contact killing leads to the formation of clonal domains, which increase in size over time. Scale bar: 50 μm. c) Relative abundance of the killer cells over time for four different initial conditions (killer cell relative abundance during inoculation: 0.5, 0.33, 0.17, 0.09, from top to bottom curve) measured from time lapse images as depicted in (b). In all cases, the relative abundance of killer cells initially increased quickly, followed by a substantially slower increase after 3 h. (See also Supplementary Video 1.)

relatively low cell concentrations ($OD_{600} = 1$). However, we began measuring the relative abundance of the fluorescent strain only after a dense cell layer has formed, which we define to be when time = 0 h, after which the vast majority of killing takes place. Killer populations

increased their relative abundance from 12-42 %. In contrast, we performed control experiments with two non-killer strains. When killing was absent, the population of the fluorescent strain changed by less than 3 % over 15 h for various mixing ratios (Supplementary Fig. S2). Therefore, demographic changes in biofilms with T6SS-active strains can mainly be attributed to killing. In all cases of unidirectional killing, the killer strain initially increased its population rapidly and reached ~ 90 % of its final size after ~ 3 h. Killing dramatically slowed afterwards. We observed similar temporal dynamics in experiments with mutually killing *V. cholerae* strains (Supplementary Fig. S4a,b, Supplementary Video 1). Again, a transition from rapid killing to almost no killing occurred after ~ 3 h. These observations are consistent with previously reported observations of small but long-lived target populations [23]. Why does T6SS-mediated killing stop after just a few hours?

B. Cell debris barrier

Surprisingly, we found that the boundary between competing strains was visible in images recorded with bright-field microscopy (Fig. 2a). Dark outlines become visible in bright-field images (Fig. 2a, top image); these dark outlines align with the interface between domains of killer and target cells in fluorescence images (Fig. 2a, bottom image). Time lapse images showed that these dark outlines form at early times in biofilms with killing, but they are absent at all times in non-killer biofilms i.e., those with two isogenic T6SS- strains (Supplementary Fig. S3). Small clonal domains still emerged in non-killer biofilms as non-motile, divided cells typically remain close after reproduction (Fig. 2b, bottom image), but the interface between these clonal domains did not appear dark in bright-field images (Fig. 2b, top image). The ability to visualize the interface between competing strains using bright-field microscopy is not expected since the two isogenic strains do not differ in their material properties—including index of refraction—so they appear identical when imaged with bright-field microscopy. The presence of dark lines in biofilms with T6SS killing suggests that there occurred a change in material properties (e.g., index of refraction) at the border between strains. Based on this observation, and the data presented above, we hypothesized that dead cell debris accumulates as cells are killed. Such cell debris may eventually prevent competing cells from contacting. Similar observations have been made previously when studying T6SS-mediated interactions with non-lethal effectors [58–60].

To test our hypothesis, we visualized dead cell debris in growing biofilms with propidium iodide (PI). PI binds to the DNA of cells with a compromised membrane and exhibits high red fluorescence. While stained dead cells appeared throughout the biofilm during the earliest stages of growth when clonal domains are small (Fig. 2c, see also Supplementary Video 2), at later times the dead cell stain was clearly localized at the interface between large clonal domains (Fig. 2d). The PI signal is well aligned with both the interface between strains and the dark outlines seen with bright-field microscopy (Fig. 2e). The PI signal exhibits a peak at the same position (distance of $6.2\,\mu$m and $31.3\,\mu$m) where the cell fluorescence declines to about 30 % of its maximum value. From a Gaussian fit we found that both peaks in PI signal and bright-field signal differ in position by less than $0.3\,\mu$m and differ in width (i.e. standard deviation of the peak) by less than $0.1\,\mu$m. This sub-micron alignment of signals suggests that dark outlines observed via bright-field microscopy correspond to a substantial amount of cell debris at the interfaces between patches.

To quantify the localization of dead cell debris at interfaces throughout the biofilm, we measured the mean intensity of PI signal as a function of distance from the interface between strains (Fig. 2f, see Supplementary for more details on the image analysis). The intensity of the PI signal decays with distance from the strain interface, and reaches half its maximum value at a distance of $1.4\,\mu$m. We applied the same image analysis to bright field images and characterized the dark outlines at the strain interfaces. The dark outlines lead to a similar decaying curve, reaching half its maximum value at a distance of about $1.8\,\mu$m (Fig. 2f) or higher, depending on the chosen threshold value during image analysis (supplementary Fig. S1c). Both curves confirm that dead cell debris is highly localized at the interface between strains. Crucially, the estimated dead cell debris layer thickness is larger than the length of a *V. cholerae* cell.

To account for the observed slow rate of killing after 3 h, the dead cell debris that separates competing strains must also be stable over long periods of time. We observed that debris from one individual dead cell remained clearly visible for at least 60 minutes, even as it was relocated via forces exerted by neighboring cells as those reproduce and die (Fig. 2g). However, the emergence of more dead cells in close proximity inhibits tracking for longer times.

To quantify the persistence of dead cell material over long times, we mixed 98 % T6SS+ killer cells and 2 % T6SS- target cells and inoculated at high density ($OD_{600} = 10$), so experiments began with close-packed cellular monolayers. Target cells were very far from each other, allowing us to isolate and track individual stained dead cells over long times (~ 10 h). All 117 individual target cells died within 1.2 h of inoculation (Fig. 2h), and were tracked by PI labeling afterwards. The number of dead cells with detectable PI signal slowly decreased over time. The decrease in the number of PI-labeled dead cells may be due to a local loss in the presence of dead cell debris, e.g., the material may degrade and diffuse away. Note that the PI-labeled area per dead cell also decreased over time (Supplementary Fig. S5), which may be caused by degradation or compaction of dead cell debris. However, despite the observed decrease of dead cell debris,

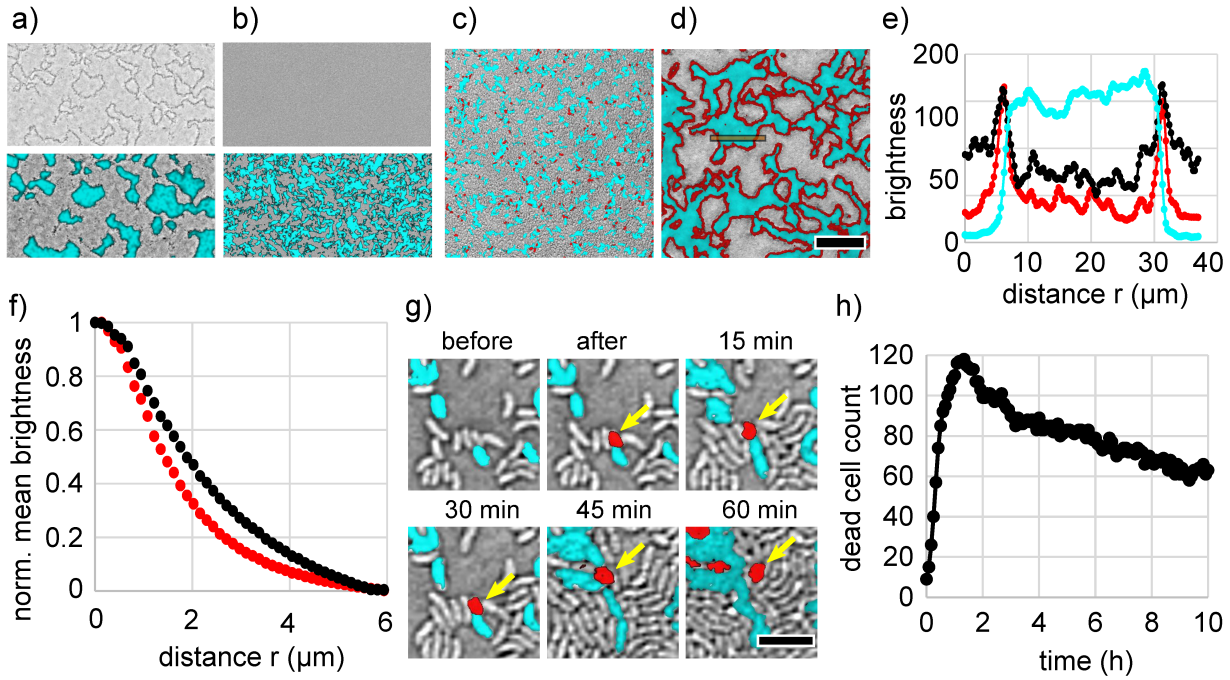

FIG. 2: Characterization of dead cell debris. a) Representative bright-field image alone (top) and overlaid with fluorescence channel (bottom) of biofilms exhibiting unidirectional killing, recorded after 7 h of growth. Killer cells express sfGFP (cyan) while target cells are unlabelled. The entire field of view is densely packed with bacteria. b) Same as (a) but the killer strain is engineered to be T6SS-deficient; no T6SS killing occurs and dark outlines are absent. c, d) Merged bright-field and fluorescence images of unidirectional killing at start (0 h) (c) and after 7 h (d). Again, the killer expresses sfGFP (visible as cyan) while the target is unlabeled (gray). The DNA of compromised cells, i.e., dead cell debris, is labelled red via PI. Scale bar (a-d): 30 μm. e) Intensity profile of different microscope images across a clonal patch (integrated vertically over the orange box in (d)) in the fluorescence images and bright-field image (inverted grey scale). f) Normalized mean intensity of PI signal (red curve) and inverted bright-field signal (black curve) within a distance r from the interface between competing strains in (d). g) Killing event, where a fluorescent killer cell kills a non-fluorescent target cell, which subsequently turns red. The dead cell debris is relocated by neighboring cells that exert forces upon growth. (Scale bar: 4 μm) h) Counting the number of discrete PI labeled cells over time demonstrates that PI-labeled dead cell debris persists long after cell death. Data were recorded from individual target cells densely surrounded by killer cells (initial target to killer number ratio of 1:50).

over 80 % of dead cells displayed a clear PI signal after 4 h, and the majority of dead cells (over 50 %) still displayed a clear PI signal after 10 h. Thus, a substantial amount of dead cell debris persisted over several hours.

We can derive a simple estimate for the time that it takes a dead cell debris barrier to form in our experiments. A single layer of dead cells is sufficient to halt killing. The time it takes a single layer of dead cells to form depends on the kill rate, which we estimate from experiments in which individual target cells are surrounded by killer cells (Fig. 2h). Target cells died after $\tau = 0.43 \pm 0.02$ h on average (N = 117 individual target cells). In a random, close-packing of non-spherical cells, each cell is expected to contact, on average, between $z = 6$ (cell monolayer, [61]) and $z = 10$ (three-dimensional, [62]) other cells. Assuming that killer cells fire the T6SS apparatus in random directions [11], a contact between killer and target cells leads to a killing event between $z \cdot \tau = 2.58 \pm 0.12$ h and 4.30 ± 0.20 h on average. This time scale agrees with our experimental finding in Fig. 1c.

Accumulation of dead cell debris is also present in competitions between non-isogenic strains. To test the accumulation of debris between non-isogenic strains, we competed the previously used *V. cholerae* killer (T6SS+) against other killer strains (four other environmental isolates of *V. cholerae* [29]) and a non-killer strain (*Vibrio harveyi*) (Supplementary Fig. S6). Moreover, we competed a killing deficient (T6SS-) variant of the *V. cholerae* strain against other T6SS+ killer strains (four other environmental isolates of *V. cholerae* and *Enterobacter cloacae* [63, 64]) to test whether debris accumulation can be independent of the toxins used by different strains (Supplementary Fig. S7). In every strain combination, we observed the signatures of killing inhibition due to dead cell debris, i.e. localized dead cell stain (PI) that aligns

with both the interface between strains as well as dark outlines in bright-field microscopy.

The evidence presented in Fig. 1 and Fig. 2 suggests that accumulated dead cell debris prevents contact between cells and thus prevents contact killing. However, these data cannot rule out counter-hypotheses such as a change in T6SS gene expression, nutrient density, or oxygen concentration. To directly test if the presence of dead cell debris hinders killing, we mechanically disturbed the structural organization of the biofilms and thus broke down dead cell debris barriers, without otherwise altering biofilm conditions (see sketch in Fig. 3a). First, we studied a co-culture of killer and target *V. cholerae* strains. We inoculated the strains at a low initial concentration ($OD_{600} = 1$) between an agar plate and a cover glass, and began the measurement after a dense layer of cells formed. Killer cells initially expanded their population; by 3 h, the expansion of killer cells halted (Fig. 3b). After 4.5 h we sheared the biofilm by rotating the cover slip with respect to the agar pad in small circular motions (diameter ~ 2 mm), until both strains and the dead cell debris were well mixed. After the perturbation, we observed an immediate increase in the fraction of killer cells indicating that killing resumed (Fig. 3b). However, the killer strain took over space almost completely and the remaining target cell domains are too small for us to observe if dead cell debris barriers formed again to separate killer and target cells.

Thus, we performed a new perturbation experiment with two 'mutual' killer *V. cholerae* strains, i.e., each strain was T6SS+ and able to kill the other strain. At 5 h, well after population changes had dramatically slowed (Fig. 3d), we sheared the biofilm (Fig. 3e), thoroughly mixing the two strains and the dead cell debris. After mixing, we observed that large clonal domains again formed over time, indicating that killing had resumed. Further, we observed that these domains became separated by dead cell debris and eventually killing again ceased (Fig. 3f). After shearing and mixing the biofilm a second time (at 19.5 h, Fig. 3g), we again observed the growth of clonal domains that eventually became separated by dead cell debris (Fig. 3h). These findings demonstrate that T6SS killing was prevented by dead cell debris barrier formation, and not by other factors such as nutrient depletion or changes in cell behavior or cell density.

We quantified the growth, and mechanical destruction, of clonal domains by measuring the characteristic length of domains, L, of the fluorescent killer strain (Fig. 3i, filled circles) (see supplementary material for details). L grows rapidly during the first ~ 3 h, and much more slowly after that time. Upon the first mixing event, L immediately drops to the size of about three cells (Fig. 3e,g). After that, L increases again, demonstrating that killing had resumed. We obtained a qualitatively similar trend when mixing the biofilm a second time, as indicated by a sudden decrease in L, followed by an increase. As a control, we measured L for a biofilm that was not mechanically perturbed. The characteristic domain length that emerges after ~ 3 h in the undisturbed biofilm increases by less than 8 % over the next 37 h (empty circles in Fig. 3h); in other words, the characteristic length of domains remains nearly constant after initial domain formation has occurred.

C. Limited invasion via contact killing

The above results show that the accumulation of dead cell debris can limit the utility of T6SS-mediated killing within biofilms. Contact killing initially eliminates opponent cells, structuring the biofilm population—but only until dead cell debris accumulates and killing nearly ceases. These observations suggest that the T6SS may have limited ability to facilitate biofilm invasion and that completely taking over a biofilm from a small number of T6SS+ cells would be unlikely. To test the ability of T6SS-facilitated invasion, we examined the behavior of single killer cells in dense environments.

We mixed 1 % fluorescent killer cells with 99 % non-fluorescent, susceptible target cells, which were otherwise isogenic to the killers. We inoculated and confined an initially dense monolayer of cells ($OD_{600} = 10$) on LB agar pads such that single killer cells were completely surrounded by target cells. We also performed control experiments in which the 1 % fluorescent cells were defective killer cells (T6SS-). We found that after 24 h of growth the final killer population was only ~ 1.5X larger than the final fluorescent defective killer control population (Fig. 4b,c). In particular, clonal domains of killer cells had a mean size of $18.9\,\mu m^2$ (standard deviation of $26.7\,\mu m^2$); defective killer control cells formed clonal domains with a mean size of $10.6\,\mu m^2$ (standard deviation of $14.9\,\mu m^2$). Thus, while killer cells expanded their population more than killing-deficient cells, they were incapable of invading the existing biofilm and eliminating their competitors.

Up to this point, all presented experiments were performed in confinement, i.e., biofilms were grown confined between an agar pad and a glass cover slip, to optimize the set-up for microscopy and exclude height-dependent differences [43, 65]. While bacteria often inhabit confined geometries in natural settings [66], it is unclear if confinement itself impacts population dynamics. Thus, we next explored contact killing in unconfined environments, by growing biofilms without a cover slip limiting their height. For both mutual and unidirectional killing, we again observed that the (stronger) killer population rapidly increases for the first 3 h, at which point killing slows substantially (Supplementary Fig. S4c,d) and a layer of dead cell debris separates competing strains.

We also repeated the experiments on expansion of single active and defective single killer cells in dense environments but without confinement. For both killer and defective killer experiments, biofilms reach a height of $92\,\mu m \pm 2\,\mu m$ after 24 h of growth. Similar to the re-

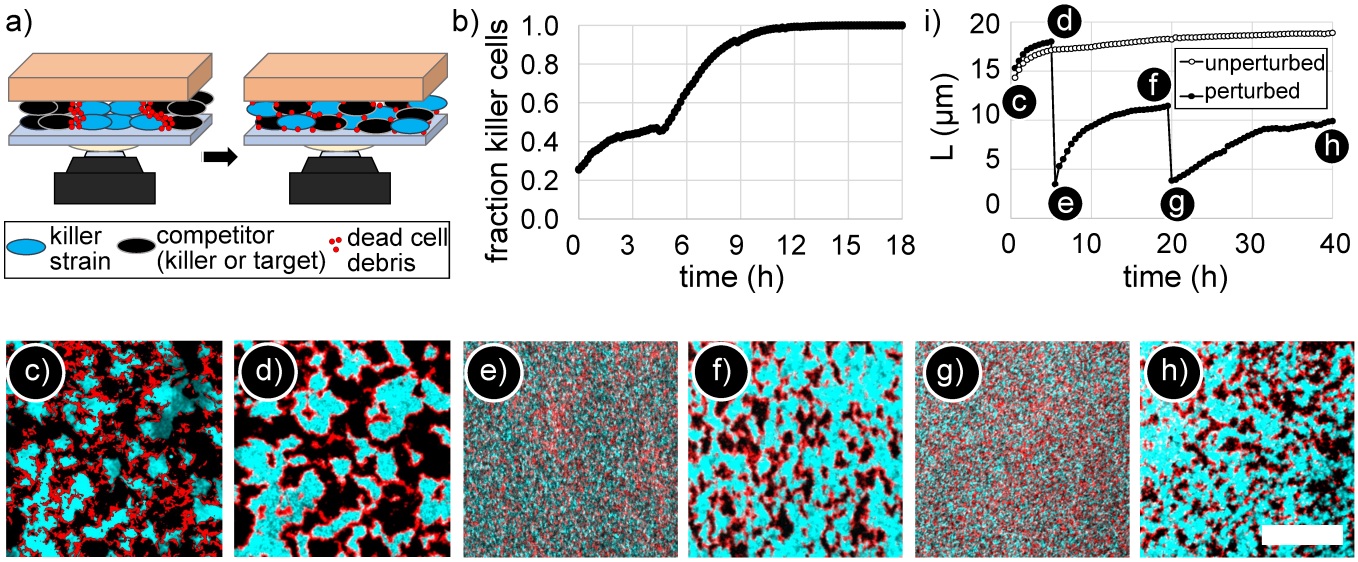

FIG. 3: Mechanical perturbation of dead cell debris barriers between domains of competing strains. (a) Sketch of mechanical perturbation experiments. The agar pad was rotated against the cover glass, mixing both strains and the dead cell debris within the biofilm. (b) For unidirectional killing (*V. cholerae* killer against target strain), the fraction of killer cells saturated after an initial increase. After mechanical perturbation at 4.5 h, the fraction of killers increased again as killing resumed, almost eliminating target cells. (See also Supplementary Video 3) (c-h) Time-lapse fluorescence images of mechanical perturbation of a mutual killer biofilm show that phase separation occurred repeatedly: (c) after a cellular monolayer has formed (d) before and (e) after the first mechanical perturbation at 5 h, (f) before and (g) after the second perturbation at 19.5 h, and (h) the final biofilm structure. In the fluorescence images, one killer strain expresses sfGFP (cyan) while the other killer strain is unlabeled (appears black). In every image, the field of view is densely packed with cells. Dead cell debris was labeled with PI (red). Scale bar (c-h): 50 μm (i) The characteristic length, L, of domains in mutual killer biofilms increases upon coarsening with time, and abruptly decreases after both mechanical perturbation events. However, L increases after each perturbation, indicating that killing resumed (filled circles). In contrast, in un-perturbed biofilms L plateaus (empty circles).

sults under confinement, the relative abundances of killer and non-killer control populations differed only slightly (Fig. 4i,j); killer strains outperformed non-killer strains by a factor of only 1.64 throughout the whole biofilm. However, we observed that killer and defective killer strains exhibit markedly different behavior near the agar surface. At the top of the unconfined biofilm, the killer population was only 1.16 times greater than the defective killer population (Fig. 4e,f). The mean size of clonal domains were 8.0 μm^2 (standard deviation 6.0 μm^2) and 7.4 μm^2 (standard deviation 4.9 μm^2) for killer cells and defective killer cells, respectively. At the bottom of the biofilm (next to agar surface), some killer cells expanded into large clonal domains (Fig. 4g); the mean diameter of clonal domains of killer cells within 4 μm of the agar surface was 115.4 μm^2 (standard deviation 146.7 μm^2). In contrast, the defective killer cells were nearly eliminated at the bottom (Fig. 4h). (Importantly, the remaining space in Fig. 4e-h is occupied by a non-killer strain lacking fluorescent proteins.) In the representative biofilm stacks shown in Fig. 4i,j, within 4 μm of the agar surface, the final population of killer cells was 270 times greater than the population of defective killer cells. Thus, although killer cells were only slightly better at invading unconfined biofilms than defective killer cells, killer cells were able to capture territory at the inoculation surface more efficiently.

It is likely that physical effects observed in studies of lateral range expansions [67–70] also play a role in the upward growth of unconfined biofilms. Previous studies found that proliferating cells in crowded environments interact mechanically [71–73], pushing cells towards the expanding cell front. In analogy, during vertical biofilm growth, the few labeled, non-killer cells may be mechanically pushed off the agar surface by neighboring cells that proliferate. These pushing forces may be diminished near dead cells, which do not reproduce, helping killer cells surrounded by dead cells to remain near the agar surface. In a related vein, it has been shown that rod-shaped bacteria at a solid-liquid interface undergo a mechanically driven transition from planar to vertical orientation during biofilm growth [74–76]. Such a transition likely also occurs in biofilms grown on agar pads. Such cellular reorientations could impact the number and extent of cell-cell contacts, thus altering the kill rate, and may also damage the debris interface. In fact, our time-

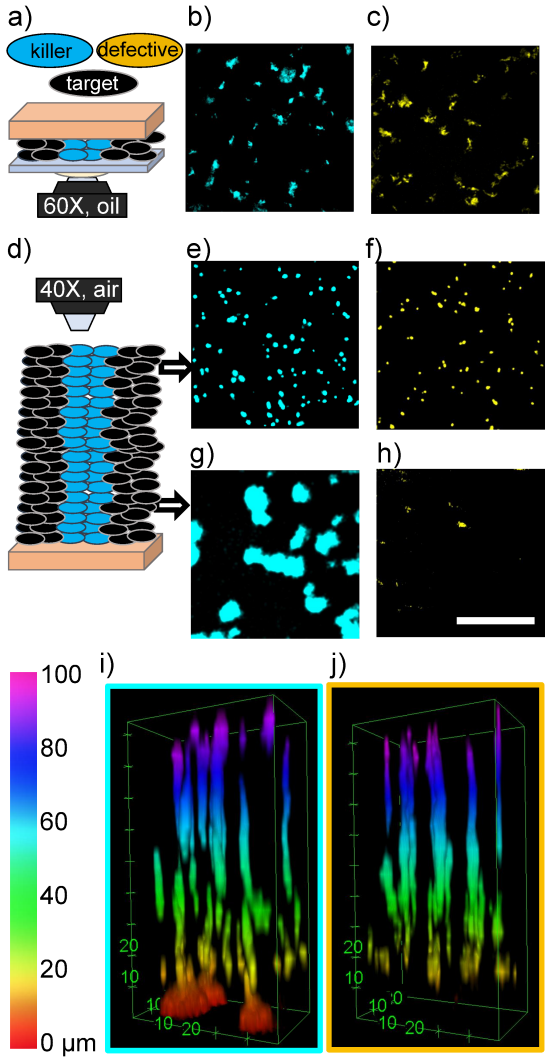

FIG. 4: Invasion of dense biofilms by individual cells imaged with confocal microscopy after 24 h of biofilm growth. Biofilms grew from a dense cell monolayer containing 1 % fluorescent cells, which were either T6SS+ killer cells (marked blue) or T6SS- defective killer cells (marked yellow). The remaining 99 % of the population were non-fluorescent target cells, appearing black. In a confined geometry (schematic in a), killer cells (b) expanded their population only ~ 1.50 times more than defective killer cells (c). In unconfined biofilms (schematic in d) the final abundance of fluorescent cells depended on the distance above the agar surface. At the top of the biofilm, killer cells (e) only expanded their population 1.16 times more than defective killer cells (f). At the bottom, the killer population (g) was 275 times larger than defective killer population (h), which was almost absent. (Scale bar b,c,e-h: 50 μm) (i,j) 3D stack of unconfined biofilms showing that killer (i) and defective killer (j) cells performed different only within the bottom $\sim 10\,\mu$m. The color bar indicates the distance from the agar pad.

lapse analysis of unconfined biofilms (supplementary Fig. S4d) shows that the relative abundances of killer cells at the top and the bottom of the biofilm was established during early stages of biofilm growth - when the structural transition likely happens - and remains unchanged afterwards. In a related vein, it was recently reported that cells near the substrate and cells above the substrate behave differently [77], which is consistent with our observations of killer cells at and above the agar surface. However, understanding the roles of mechanical pushing and cellular reorganization in detail would require single cell resolution experiments, which is beyond the scope of this work.

D. Phase separation dynamics

Finally, we analyzed the 'coarsening' behavior of clonal domains during the mechanical shearing experiments (Fig. 3c-i). Previous works predicted that the observed phase separation is part of the broad Model A, or Model A', universality class [24, 28]. As a result, the characteristic domain length, L, is predicted to scale as $L \sim \sqrt{t}$ with time t. The mean structure factor, S_L, scales as $S_L \sim t$ [24]. Here, we confirm that killing-mediated phase separation follows these dynamics, despite the accumulation of a dead cell debris barrier (Fig. 5). Following the analysis in [24], we calculated the Fourier-transformed structure factor, $S(q)$, which provides a measure for the frequency of structure sizes with wavenumber q. We determined the characteristic wavenumber, q_m, as the mean wavenumber q weighted by $S(q)$. From this, we obtained the characteristic domain length, L, which is inversely proportional to q_m, and the mean structure factor S_L, which is the height of $S(q)$ at q_m (see supplementary methods for details). S_L exhibits linear behavior each time phase separation occurs (Fig. 5a). However, all three curves exhibit a kink, where the slope decreases by a factor of 31, 9 or 4, respectively. This indicates a change in the speed of domain coarsening, likely caused by the establishment of debris barriers. We further found that L follows a square root scaling with time (Fig. 5b) at early times after both perturbation events. However, this scaling analysis depends on when we set time $t = 0$, which is experimentally ambiguous and moreover changes as the speed of coarsening decreases. This ambiguity with respect to time can be avoided by plotting S_L versus L. As predicted, it follows the time-independent, universal scaling of $S_L \sim L^2$ for all data in the mechanical shearing experiment (Fig. 5c).

III. DISCUSSION

Microbial antagonism is common in biofilms [4], and many mechanisms exist that kill on contact. Contact killing has previously been proposed to virtually eliminate susceptible competitor cells of similar numbers

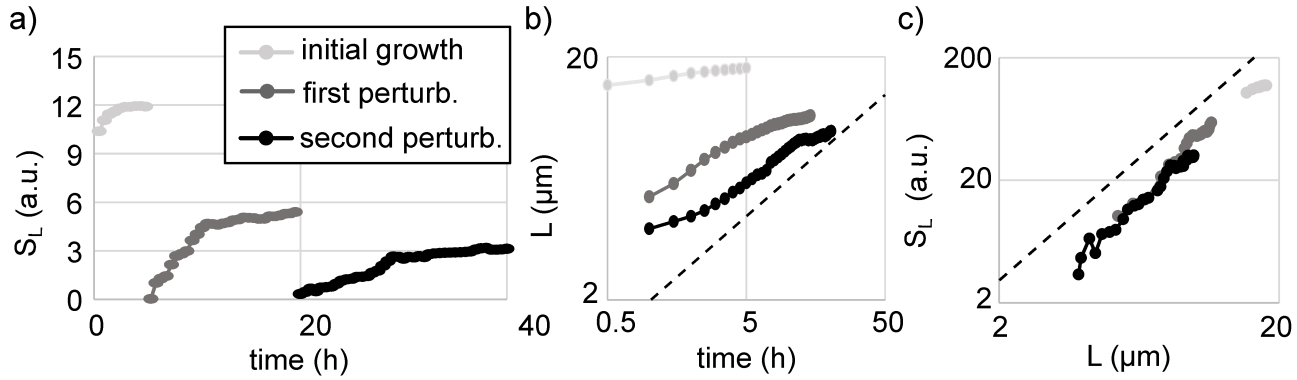

FIG. 5: Structural analysis of repeated phase separation during the perturbation experiment in Fig. 3c-i. Time-dependence of a) the mean structure factor S_L and b) the characteristic domain length L. c) Time-independent structural analysis, S_L versus L, for each recurrence of coarsening (with same color code as in (a)). Dashed lines indicate the slope that corresponds to model A coarsening.

within a few hours [9, 29, 31, 78, 79] (unless target cells reproduce sufficiently quickly [26]). Surprisingly, we found that killing-induced changes in the target population dramatically slow after approximately 3 h, independent of the initial or final relative abundances of killer cells, and independent from the final amount of contact between competing strains (which varies by a factor of 25 across the different cases explored in Fig. 1c). In fact, even when the T6SS-proficient strain had captured over 99% of the population, small domains of target cells, only a few microns in size, persisted for hours (top curve in Fig. 1c).

In this work, we focused on dead cells, finding that the accumulation of dead cell debris is responsible for the observed dramatic decrease in contact killing. By mechanically shearing biofilms, we directly show that killing resumes once dead cell debris barriers are destroyed. Shearing only modifies the positions of cells and dead cell debris, excluding many other hypotheses (such as changes in T6SS gene expression, target cell susceptibility, or metabolic activity). We further demonstrate that despite the formation of dead cell barriers the killing-mediated phase separation of competing strains still exhibits dynamics of the Model A universality class, which has been predicted previously [24, 28].

At first sight, findings presented here might appear to disagree with conclusions drawn from T6SS competition assays, in which T6SS killing decreases the abundance of target cells by several orders of magnitude [7, 13, 15, 29, 31]. However, killing competition assays often start with a majority of killer cells over target cells, and the final abundance of target cells has a non-linear relationship with the initial abundance of killer cells. Decreasing the initial abundance of killer cells leads to enhanced survival of the target cells [23]. This nonlinear phenomenon agrees with our microscopy results; we found that for the same pair of strains, target inhibition can be as high as 99.97 % (three orders of magnitude) or as low as 79.47 % (less than one order of magnitude) as the fraction of killer cells during inoculation was varied from 0.50 to 0.09, respectively. In fact, despite the excess of killer cells in competition assays, the target strain is rarely, if ever, *completely* eliminated [7, 13, 15, 29, 31]. Previous time-lapse competition assays found that the number of surviving target cells remains remarkably constant after a quick decline in the first few hours [23], consistent with the temporal dynamics we observed via microscopy. Therefore, our observations are in agreement with and explain results from previously reported competition assays. Combined, these results demonstrate that the killing efficiency must be studied and discussed in context, with the initial abundances considered. For example, traditional competition assays show that, for some strains, a large number of killer cells can kill a small number of target cells effectively, but they do not show how a small number of killer cells would perform against a large number of target cells.

Even though the efficacy of killing may be limited by the accumulation of dead cell debris, the utility remains quite high. First, it initially facilitates the formation of clonal domains. Depending on the diffusion length of secreted goods [80], this initial domain formation may be sufficient to favor intra-strain cooperation [24, 81, 82] or reciprocal benefits between different strains [2, 83]. Second, killing can prevent social cheaters from emerging in a population. Such 'policing' effects have been observed in cases where social behavior is linked with T6SS regulation [84]. Finally, we found that contact-killing strains are able to capture and maintain territory near the surface on which they were inoculated; killing-deficient cells have a much lower probability of remaining near the surface. Occupying nutrient rich territories may have long term benefits, beyond the scope of our experiments [85].

The physical inhibition of killing observed here is comparable to other phenomena as seen in contact dependent growth inhibition experiments [86]. Such a passive defense is starkest in scenarios where the target strain cannot fight back, but the accumulation of

dead cell debris eventually prevents killing and protects the target strain from elimination. Such physical protection stands in stark contrast with active, species-dependent defense mechanisms that are controlled genetically [36, 38, 40, 41]. Physical barriers represent an emergent first line of defense that do not require active sensing or control and are species independent. Other defense mechanisms, e.g. immunity proteins acquired through horizontal gene transfer [87], may help protect small numbers of target cells and become relevant if cells touch directly, e.g. before the debris barrier forms or after the debris barrier is broken down.

In this vein, it is important to note that the efficacy of T6SS killing, and thus potentially the role of debris accumulation, can vary among different combinations of strains [88]. In fact, previous measurements demonstrated that the killing ability of *V. cholerae* strains in traditional competition assays can vary by one to seven orders of magnitudes [29]. These observations suggest that T6SS killing may be highly effective in some but not all scenarios. The results presented here suggest that the efficacy of T6SS killing also depends on the stability of the cell debris barrier and the rate at which cells can overcome the barrier. The barrier may be broken down through the predation and consumption of dead cells [89], by secreted enzymes (such as lipases or DNases), by shear flow [90] or other mechanical perturbations, among other potential mechanisms. The rate at which dead cell debris breaks down may also be impacted by the chemical environment and the action of the delivered toxins [88, 91], which are known to exhibit a wide range of effects from growth inhibition to lysis [20, 21, 35, 92, 93]. Further, while we observed similar characteristics of cell debris accumulation across different co-culture competitions containing *V. cholerae*, *E. cloacae*, and *V. harveyi*, the material and physical characteristics of dead cell debris may vary across different combinations of competing strains or species, impacting how long accumulated cell debris prevents contact killing. For example, if competing strains grow at different rates, reproduction may allow the faster growing strain to push through the barrier. Further, motility may enable cells to penetrate barriers as well.

Yet, while several mechanisms may make the debris barrier less stable, dead cell debris is always an obstacle as dead bacteria do not instantaneously disappear. The relative ability or inability of dead cell debris to inhibit contact killing is not a question of if this effect is present, but instead depends on the time scale on which dead cell debris accumulates and how long debris barriers persist. In other words, while the steric hindrance by dead cell debris is likely quite general, the impact of debris barriers is specific to the experimental or ecological details [88].

The accumulation of dead cell debris and barrier formation may hold wide ranging consequences in a variety of contexts. We observe that dead cell debris facilitates the *coexistence* of antagonistic strains, including allowing killer cells to coexist with non-killer strains that cannot fight back. This concept may apply to other modes of microbial killing [4], such as killing mechanisms that act over longer distances via diffusible deadly biomolecules [94], phages [95] and bacteriocins [96]. These killing mechanisms will typically only be effective within some diffusion length. Killing may thus be hindered if a dead cell debris barrier longer than the diffusion length forms. Moreover, dead cells locally alter the chemical and material composition, promoting biofilm dispersal [97], providing a source of nutrients [98], or protecting against antibiotics [99, 100]. Finally, the phenomena we observe are reminiscent of territorial resource competition seen in a variety of ecosystems at various scales [101]. Previous models have suggested that such effects play important roles in maintaining diversity [102, 103]. Specifically, the barrier formation we observe is similar to gap formation that occurs during competition between plants [104, 105].

In conclusion, it is striking that contact killing indirectly facilitates the coexistence of antagonistic strains [106]. These results suggest that the T6SS, and perhaps other contact killing mechanisms, may not always prompt a microbial 'arms race'. Instead, T6SS-mediated killing may also stabilize diverse communities and the increase in dead cell biomass may facilitate bacterial interaction and survival against external attacks. Further, these results align with recent works which question the ecological purpose of bacterial production of antibiotics [85, 107]. Nevertheless, the fact that contact killing facilitates coexistence suggests that the impact of the T6SS in bacterial consortia is complex, and the T6SS is more than simply a potent weapon.

AUTHOR'S CONTRIBUTION

G.S. and P.Y. designed the study. C.C. and S.L.N. engineered mutant strains and prepared liquid cultures. G.S. carried out experiments and analyzed the data. G.S. and P.Y. wrote the manuscript. All authors gave feedback during project development, reviewed the manuscript, and gave final approval for publication.

FUNDING

GS is grateful for funding from the German National Academy of Sciences Leopoldina (LDPS 2017-03). BKH acknowledges funding from the Gordon and Betty Moore Foundation (Grant No. 6790.13), the School of Biological Sciences Abell Fellowship, and the College of Sciences Cullen Peck Scholars Award. PJY acknowledges funding from the Coulter Foundation and the Georgia CTSA. PJY and BKH acknowledge funding from the NSF Biomaterials (BMAT-2003721).

DATA ACCESSIBILITY

All experimental data sets are available at https://osf.io/vhmdn .

REFERENCES

[1] W. Liu, S. Jacquiod, A. Brejnrod, J. Russel, M. Burmølle, and S. J. Sørensen, ISME J. **13**, 3054 (2019).
[2] C. D. Nadell, K. Drescher, and K. R. Foster, Nat Rev Microbiol. **14**, 589 (2016).
[3] D. Yanni, P. Márquez-Zacarías, P. J. Yunker, and W. C. Ratcliff, Curr Biol. **29**, R545 (2019).
[4] E. T. Granato, T. A. Meiller-Legrand, and K. R. Foster, Curr Biol. **29**, R521 (2019).
[5] L. García-Bayonaand L. E. Comstock, Science **361**, eaat2456 (2018).
[6] S. K. Aoki, R. Pamma, A. D. Hernday, J. E. Bickham, B. A. Braaten, and D. A. Low, Science **309**, 1245 (2005).
[7] S. Pukatzki, A. T. Ma, D. Sturtevant, B. Krastins, D. Sarracino, W. C. Nelson, J. F. Heidelberg, and J. J. Mekalanos, Proc Natl Acad Sci USA. **103**, 1528 (2006).
[8] E. Nudleman, D. Wall, and D. Kaiser, Science **309**, 125 (2005).
[9] D. P. Souza, G. U. Oka, C. E. Alvarez-Martinez, A. W. Bisson-Filho, G. Dunger, L. Hobeika, N. S. Cavalcante, M. C. Alegria, L. R. S. Barbosa, R. K. Salinas, C. R. Guzzo, and C. S. Farah, Nat Commun. **6**, 6453 (2015).
[10] L. E. H. Bingle, C. M. Bailey, and M. J. Pallen, Curr Opin Microbiol. **11**, 3 (2008).
[11] M. Basler, M. Pilhofer, G. P. Henderson, G. J. Jensen, and J. J. Mekalanos, Nature **483**, 182 (2012).
[12] L. Lin, E. Lezan, A. Schmidt, and M. Basler, Nat Commun. **10**, 2584 (2019).
[13] F. R. Cianfanelli, L. Monlezun, and S. J. Coulthurst, Trends Microbiol. **24**, 51 (2016).
[14] B. T. Ho, T. G. Dong, and J. J. Mekalanos, Cell Host Microbe **15**, 9 (2014).
[15] S. S. Watve, J. Thomas, and B. K. Hammer, Plos One **10**, 0138834 (2015).
[16] A. Zoued, Y. R. Brunet, E. Durand, M.-S. Aschtgen, L. Logger, B. Douzi, L. Journet, C. Cambillau, and E. Cascales, Biochim Biophys Acta. **1843**, 1664 (2014).
[17] A. Filloux, A. Hachani, and S. Bleves, Microbiology **154**, 1570 (2008).
[18] P. G. Leiman, M. Basler, U. A. Ramagopal, J. B. Bonanno, J. M. Sauder, S. Pukatzki, S. K. Burley, S. C. Almo, and J. J. Mekalanos, Proc Natl Acad Sci USA. **106**, 4154 (2009).
[19] A. Joshi, B. Kostiuk, A. Rogers, J. Teschler, S. Pukatzki, and F. H. Yildiz, Trends Microbiol. **25**, 267 (2017).
[20] C. V. Crisanand B. K. Hammer, Environ Microbiol. **00**, 10.1111/1462-2920.14976 (2020).
[21] A. B. Russell, S. B. Peterson, and J. D. Mougous, Nat Rev Microbiol **12**, 137 (2014).
[22] S. Schwarz, R. D. Hood, and J. D. Mougous, Trends Microbiol. **18**, 531 (2010).
[23] D. L. MacIntyre, S. T. Miyata, M. Kitaoka, and S. Pukatzki, Proc Natl Acad Sci USA. **107**, 19520 (2010).
[24] L. McNally, E. Bernardy, J. Thomas, A. Kalziqi, J. Pentz, S. P. Brown, B. K. Hammer, P. J. Yunker, and W. C. Ratcliff, Nat Commun. **8**, 14371 (2017).
[25] N. Vallespir Loweryand T. Ursell, Proc Natl Acad Sci USA. **116**, 379 (2019).
[26] D. B. Borenstein, P. Ringel, M. Basler, and N. S. Wingreen, PLoS Comput Biol. **11**, e1004520 (2015).
[27] A. Kalziqi, S. L. Ng, D. Yanni, G. Steinbach, B. K. Hammer, and P. J. Yunker, Viscosity independent diffusion mediated by death and reproduction in biofilms (2019).
[28] M. O. Lavrentovichand D. R. Nelson, Phys Rev E. **100**, 042406 (2019).
[29] E. E. Bernardy, M. A. Turnsek, S. K. Wilson, C. L. Tarr, and B. K. Hammer, Appl Environ Microbiol. **82**, 2833 (2016).
[30] C. V. Crisan, A. T. Chande, K. Williams, V. Raghuram, L. Rishishwar, G. Steinbach, S. S. Watve, P. Yunker, I. K. Jordan, and B. K. Hammer, Genome Biol. **20**, 163 (2019).
[31] J. Zheng, B. Ho, and J. J. Mekalanos, Plos One **6**, e23876 (2011).
[32] J. Vacheron, M. Péchy-Tarr, S. Brochet, C. M. Heiman, M. Stojiljkovic, M. Maurhofer, and C. Keel, ISME J. **13**, 1318 (2019).
[33] A. J. Verster, B. D. Ross, M. C. Radey, Y. Bao, A. L. Goodman, J. D. Mougous, and E. Borenstein, Cell Host Microbe **22**, 411 (2017).
[34] S. J. Coulthurst, Res Microbiol. **164**, 640 (2013).
[35] A. B. Russell, M. LeRoux, K. Hathazi, D. M. Agnello, T. Ishikawa, P. A. Wiggins, S. N. Wai, and J. D. Mougous, Nature **496**, 508 (2013).
[36] S. J. Hersch, N. Watanabe, M. S. Stietz, K. Manera, F. Kamal, B. Burkinshaw, L. Lam, A. Pun, M. Li, A. Savchenko, and T. G. Dong, Nature Microbiology **5**, 706 (2020).
[37] S. T. Miyata, D. Unterweger, S. P. Rudko, and S. Pukatzki, PLoS pathogens **9**, e1003752 (2013).
[38] J. Toska, B. T. Ho, and J. J. Mekalanos, Proceedings of the National Academy of Sciences of the United States of America **115**, 7997 (2018).
[39] M. Basler, B. Ho, and J. Mekalanos, Cell **152**, 884 (2013).
[40] T. G. Dong, S. Dong, C. Catalano, R. Moore, X. Liang, and J. J. Mekalanos, Proceedings of the National

Academy of Sciences **112**, 2181 (2015).
[41] B. Lories, S. Roberfroid, L. Dieltjens, D. De Coster, K. R. Foster, and H. P. Steenackers, Current Biology **30**, 1231 (2020).
[42] H. A. S. Nair, S. Periasamy, L. Yang, S. Kjelleberg, and S. A. Rice, J Biol Chem. **292**, 477 (2017).
[43] X. Wang, G. Wang, and M. Hao, Comput Math Method M. **2015**, 581829 (2015).
[44] E. J. Wentland, P. S. Stewart, C.-T. Huang, and G. A. McFeters, Biotechnol Prog. **12**, 316 (1996).
[45] K. D. Xu, P. S. Stewart, F. Xia, C.-T. Huang, and G. A. McFeters, Appl Environ Microbiol. **64**, 4035 (1998).
[46] H. Anwar, J. L. Strap, and J. W. Costerton, Antimicrob Agents Chemother. **36**, 1347 (1992).
[47] M. Bartolini, S. Cogliati, D. Vileta, C. Bauman, L. Rateni, C. Leñini, F. Argañaraz, M. Francisco, J. M. Villalba, L. Steil, U. Völker, and R. Grau, J Bacteriol. **201**, e00473 (2018).
[48] M. Bartolini, S. Cogliati, D. Vileta, C. Bauman, L. Rateni, C. Leñini, F. Argañaraz, M. Francisco, J. M. Villalba, L. Steil, U. Völker, and R. Grau, J Bacteriol. **201**, e00473 (2019).
[49] T. M. Brooks, D. Unterweger, V. Bachmann, B. Kostiuk, and S. Pukatzki, Journal of Biological Chemistry **288**, 7618 (2013).
[50] E. Altindis, T. Dong, C. Catalano, and J. Mekalanos, mBio **6**, e00075 (2015).
[51] T. G. Dong, B. T. Ho, D. R. Yoder-Himes, and J. J. Mekalanos, Proceedings of the National Academy of Sciences **110**, 2623 (2013).
[52] R. D. Hood, P. Singh, F. Hsu, T. Güvener, M. A. Carl, R. R. S. Trinidad, J. M. Silverman, B. B. Ohlson, K. G. Hicks, R. L. Plemel, M. Li, S. Schwarz, W. Y. Wang, A. J. Merz, D. R. Goodlett, and J. D. Mougous, Cell Host Microbe **7**, 25 (2010).
[53] A. Hachani, N. S. Lossi, and A. Filloux, J Vis Exp. , e50103 (2013).
[54] S. R. Church, T. Lux, C. Baker-Austin, S. P. Buddington, and S. L. Michell, PLoS One **11**, e0165500 (2016).
[55] T. Ishikawa, D. Sabharwal, J. Bröms, D. L. Milton, A. Sjöstedt, B. E. Uhlin, and S. N. Wai, Infect Immun. **80**, 575 (2012).
[56] T. L. Czárán, R. F. Hoekstra, and L. Pagie, Proc Natl Acad Sci USA. **99**, 786 (2002).
[57] T. L. Czaranand R. F. Hoekstra, Proc R Soc Lond Biol. **270**, 1373 (2003).
[58] M. Wong, X. Liang, M. Smart, L. Tang, R. Moore, B. Ingalls, and T. G. Dong, Appl Environ Microbiol. **82**, 6881 (2016).
[59] M. A. Zepeda-Rivera, C. C. Saak, and K. A. Gibbs, J Bacteriol. **200**, e00688 (2018).
[60] L. M. Wenren, N. L. Sullivan, L. Cardarelli, A. N. Septer, and K. A. Gibbs, mBio **4**, 10.1128/mBio.00374-13 (2013).
[61] G. Delaney, D. Weaire, S. Hutzler *, and S. Murphy, Philosophical Magazine Letters **85**, 89 (2005).
[62] A. Donev, I. Cisse, D. Sachs, E. A. Variano, F. H. Stillinger, R. Connelly, S. Torquato, and P. M. Chaikin, Science **303**, 990 (2004).
[63] W. Z. Stephens, A. R. Burns, K. Stagaman, S. Wong, J. F. Rawls, K. Guillemin, and B. J. M. Bohannan, ISME J. **10**, 644 (2016).
[64] B. H. Schlomann, T. J. Wiles, E. S. Wall, K. Guillemin, and R. Parthasarathy, Proc Natl Acad Sci USA. **116**, 21392 (2019).
[65] R. S. Renslow, P. D. Majors, J. S. McLean, J. K. Fredrickson, B. Ahmed, and H. Beyenal, Biotechnol Bioeng **106**, 928 (2010).
[66] Y. M. Bar-On, R. Phillips, and R. Milo, Proc Natl Acad Sci USA. **115**, 6506 (2018).
[67] C. F. Schreck, D. Fusco, Y. Karita, S. Martis, J. Kayser, M.-C. Duvernoy, and O. Hallatschek, bioRxiv , 743534 (2019).
[68] A. Giometto, D. R. Nelson, and A. W. Murray, Proceedings of the National Academy of Sciences **115**, 11448 (2018).
[69] O. Hallatschek, P. Hersen, S. Ramanathan, and D. R. Nelson, Proc. Nat. Acad. Sci. **104**, 19926 (2007).
[70] F. D. Farrell, M. Gralka, O. Hallatschek, and B. Waclaw, Journal of The Royal Society Interface **14**, 20170073 (2017).
[71] A. Kalziqi, D. Yanni, J. Thomas, S. L. Ng, S. Vivek, B. K. Hammer, and P. J. Yunker, Phys Rev Lett. **120**, 018101 (2018).
[72] K. Copenhagen, R. Alert, N. S. Wingreen, and J. W. Shaevitz, **arXiv:2001.03804** (2020).
[73] J. Yan, A. G. Sharo, H. A. Stone, N. S. Wingreen, and B. L. Bassler, Proc Natl Acad Sci USA. **113**, E5337 (2016).
[74] J. Yan, A. G. Sharo, H. A. Stone, N. S. Wingreen, and B. L. Bassler, Proceedings of the National Academy of Sciences **113**, E5337 (2016).
[75] F. Beroz, J. Yan, Y. Meir, B. Sabass, H. A. Stone, B. L. Bassler, and N. S. Wingreen, Nat Phys. **14**, 954 (2018).
[76] K. Drescher, J. Dunkel, C. D. Nadell, S. van Teeffelen, I. Grnja, N. S. Wingreen, H. A. Stone, and B. L. Bassler, Proceedings of the National Academy of Sciences of the United States of America **113**, E2066 (2016).
[77] B. Qin, C. Fei, A. A. Bridges, A. A. Mashruwala, H. A. Stone, N. S. Wingreen, and B. L. Bassler, Science **369**, 71 (2020).
[78] S. Coulthurst, Microbiology **165**, 503 (2019).
[79] C. Chen, X. B. Yang, and X. H. Shen, Front Microbiol. **10**, 1484 (2019).
[80] A. D. Co, S. v. Vliet, D. J. Kiviet, S. Schlegel, and M. Ackermann, Nat Ecol Evol. , 1 (2020).
[81] T. Julou, T. Mora, L. Guillon, V. Croquette, I. J. Schalk, D. Bensimon, and N. Desprat, Proc Natl Acad Sci USA. **110**, 12577 (2013).
[82] A. Dobay, H. C. Bagheri, A. Messina, R. Kümmerli, and D. J. Rankin, J Evol Biol. **27**, 1869 (2014).
[83] B. Momeni, A. J. Waite, and W. Shou, eLife **2**, e00960 (2013).
[84] C. Majerczyk, E. Schneider, and E. P. Greenberg, eLife **5**, e14712 (2016).
[85] M. E. Hibbing, C. Fuqua, M. R. Parsek, and S. B. Peterson, Nat Rev Microbiol **8**, 15 (2010).
[86] M. J. Bottery, I. Passaris, C. Dytham, A. J. Wood, and M. W. van der Woude, Curr Biol. **29**, 3622 (2019).
[87] J. Thomas, S. S. Watve, W. C. Ratcliff, and B. K. Hammer, mBio **8**, e00654 (2017).
[88] W. P. J. Smith, A. Vettiger, J. Winter, T. Ryser, L. E. Comstock, M. Basler, and K. R. Foster, PLOS Biology **18**, e3000720 (2020).
[89] J. Pérez, A. Moraleda-Muñoz, F. J. Marcos-Torres, and J. Muñoz-Dorado, Environ Microbiol. **18**, 766 (2016).
[90] P. Thomen, J. Robert, A. Monmeyran, A.-F. Bitbol, C. Douarche, and N. Henry, PLoS One **12**, e0175197

(2017).
[91] D. Unterweger, S. T. Miyata, V. Bachmann, T. M. Brooks, T. Mullins, B. Kostiuk, D. Provenzano, and S. Pukatzki, Nat Commun. **5**, 3549 (2014).
[92] E. Durand, C. Cambillau, E. Cascales, and L. Journet, Trends Microbiol. **22**, 498 (2014).
[93] X. Yang, M. Long, and X. Shen, Molecules **23**, 1009 (2018).
[94] M. A. Kohanski, D. J. Dwyer, and J. J. Collins, Nat Rev Microbiol **8**, 423 (2010).
[95] K. E. Kortright, B. K. Chan, J. L. Koff, and P. E. Turner, Cell Host Microbe **25**, 219 (2019).
[96] D. Scholl, Annu Rev Virol. **4**, 453 (2017).
[97] A. Mai-Prochnow, F. Evans, D. Dalisay-Saludes, S. Stelzer, S. Egan, S. James, J. S. Webb, and S. Kjelleberg, Applied and Environmental Microbiology **70**, 3232 (2004).
[98] S. J. Schink, E. Biselli, C. Ammar, and U. Gerland, Cell Systems **9**, 64 (2019).
[99] Z. Podlesek, M. Butala, A. Šakanović, and D. Žgur Bertok, Antonie van Leeuwenhoek **109**, 523 (2016).
[100] T. M. Auschill, N. B. Arweiler, L. Netuschil, M. Brecx, E. Reich, and A. Sculean, Archives of oral biology **46**, 471 (2001).
[101] J. Wuand O. L. Loucks, The Quarterly Review of Biology **70**, 439 (1995).
[102] B. G. Weiner, A. Posfai, and N. S. Wingreen, Proceedings of the National Academy of Sciences **116**, 17874 (2019).
[103] P. Amarasekare, Ecology Letters **6**, 1109 (2003).
[104] J. Liao, J. Bogaert, and I. Nijs, Scientific Reports **5**, 11229 (2015).
[105] N. V. L. Brokaw, Chapter 4 - treefalls, regrowth, and community structure in tropical forests, in *The Ecology of Natural Disturbance and Patch Dynamics*, edited by S. T. A. Pickettand P. S. White (Academic Press, San Diego, 1985) pp. 53–69.
[106] C. Ratzke, J. Barrere, and J. Gore, Nat Ecol Evol. **4**, 376–383 (2020).
[107] G. Pishchanyand R. Kolter, Mol Microbiol. **113**, 580–587 (2020).